UDC 533.7 :533.6.011.8

TECHNICAL REPORT OF NATIONAL AEROSPACE LABORATORY

TR-192T

Transient Couette Flow of Rarefied Binary Gas Mixtures

Katsuhisa KOURA

March 1970

NATIONAL AEROSPACE LABORATORY

CHŌFU, TOKYO, JAPAN

List of NAL Technical Reports

TR-171T Simple Flow Characteristics Across a Strong Shock Wave	Kenneth K. YOSHIKAWA	Feb. 1969
TR-172 Measurements of Dynamic Stability Derivatives of Cones and Delta-Wings at High Speed	Mitsunori YANAGIZAWA	Feb. 1969
TR-173T The Coupling Effect of Radiative Heat on Convective Heat Transfer	Kenneth K. YOSHIKAWA	Feb. 1969
TR-174 Difference Method for Navier-Stokes Equation	Hajime MIYOSHI	Apr. 1969
TR-175 Stalling Characteristics of the NACA 0012 Aerofoil Section at Low Reynolds Numbers	Yasuharu NAKAMURA, Kōji ISOGAI & Hiroshi EJIRI	Jun. 1969
TR-176 On the Vibration of Axial-flow Turbomachine Blades (I) Natural Frequency, Mode and Vibratory Stress Distribution	Toshio MIYACHI, Shoji HOSHIYA, Yasuyuki SOFUE, Saburo AMIHOSHI, Tadasuke IWABU & Katsumi TAKEDA	Jul. 1969
TR-177 Thrust Magnitude Control of Solid Rocket Motors —Characteristics Analysis and Small Motor Tests—	Tomifumi GODAI, Yoshinori YUZAWA, Katsuya ITO & Hisao NISHIMURA	Jul. 1969
TR-178 Necessary Conditions for the Optimal Weighting Matrices of Quadratic Performance Index to Maximize the Measure of the Controllable Set	Nagakatsu KAWAHATA	Jul. 1969
TR-179 Measurements of Transient Ablation of Teflon	Shigeaki NOMURA	Aug. 1969
TR-180 Measurement and Analysis of Atmospheric Turbulence over the SUZUKA Mountain Range	Kazuyuki TAKEUCHI, Kōichi ONO, Kōsaburo YAMANE, Tōichi OKA & Tokuo SOTOZAKI	Aug. 1969
TR-181 Unsteady Surface Pressure on an Oscillating Aerofoil at High Mean Angles of Attack with Special Reference to Stall Flutter	Yasuharu NAKAMURA, Kōji ISOGAI, & Hiroshi EJIRI	Aug. 1969
TR-182 On the Natural Viblation of Plates Restrained at Several Points	Taketoshi HANAWA, Yasuo TADA, Hideo IZUMI & Shinichi KOSHIDE	Sep. 1969
TR-183 Experimental Investigation of Strength of Axial Flow Compressor Blade Root —Pin Joints Lug having Clearance between Pin and Pin Hole—	Tameji IKEDA & Takashi YAMAGISHI	Sep. 1969
TR-184T An Inproved Method of Designing and Calculating the Minimal Wave Drag Configuration by Supersonic and Moment-of-Area Rules	Kenneth K. Yoshikawa	Oct. 1969
TR-185 Thermal Characteristics of FPR Rocket Nosecone	Kōichi OGAWA, Shinji ENDO	Nov. 1969
TR-186 The Analysis on Transmission-Line Rocket Antennas	Johji TABATA, Yoshio SAKURAI, Masao MIURA, Yoshitsugu MATSUZAKI & Norio TSUKAMOTO	Dec. 1969
TR-187 A Magnetic Attitude Measuring Instrument Applying the Holl Effect	Shigeru KIMURA, Johji TABATA & Yoshitsugu MATSUZAKI	Dec. 1969
TR-188 Analysis of Anisoelastic Errors of a Floated Single Degree of-Freedom Integrating	Masao OTSUKI, Hirokimi SHINGU, Johji TABATA, Takao SUZUKI & Shigeharu ENKYO	Jan. 1970

Transient Couette Flow of Rarefied Binary* Gas Mixtures

By

Katsuhisa KOURA**

ABSTRACT

The transient Couette flow problem of rarefied binary gas mixtures is studied for the nonlinear case, $M_i \geqslant 1$: one of the plates with equal plate temperatures is accelerated impulsively. The method of solution is the Monte Carlo method. The physical space is divided into macroscopically small cells. The change in the distribution function in a cell during a time interval Δt, which should be sufficiently small in comparison with the characteristic times $(\tau_D)_{ia}$, $(\tau_F)_{ia}$, and $(\tau_C)_{ij}$, is obtained by following the test particles for each molecular event through the event; i.e., molecular drift, external force, or molecular collision. The flow field is calculated for Maxwellian molecules and the range of Knudsen number $K_n \geqslant 0.1$ (from free molecular to transition flow regime). The relaxation phenomena of a gas mixture with the boundary effects are observed. Of particular interest are an epochal relaxation due to the molecule-surface collision and the temperature "overshoot" near the moving plate. The steady-state solutions, which are obtained from the long-time results, are also presented. The effects of Knudsen number, mixture ratio, and gas-surface interaction are investigated, and the separation phenomena between the species are observed.

1. INTRODUCTION

The transient Couette flow of rarefied binary gas mixtures has some peculiar features. In the case of no boundaries, as Grad previously noted,[1] there is an epochal relaxation*** due to the molecule-molecule collision for a disparate-mass gas mixture. When the boundary exists, there is a time scale representing the molecule-surface collision, e.g., in the case of Couette flow problem, the time for a molecule to cross the channel $t_{Di}=d/(2R_iT_0)^{\frac{1}{2}}$ plays an important role when the gas is rarefied. The result of this analysis indicates an epochal relaxation due to the molecule-surface collision. The macroscopic quantities of each species separate from each other, since the effect of the plate velocity U comes through the Mach number of the individual species $M_i=U/(\gamma R_iT_0)^{\frac{1}{2}}$ when the gas is rarefied.

To the best of the author's knowledge, the transient Couette flow problem has been solved only by Huang and Giddens[2] for the linearized simple gas case and by Koura[3] for the nonlinear simple gas case. Huang and Giddens found the velocity "overshoot" for the case of accelerating two plates in opposite directions, and Koura found the temperature "overshoot" for the case of accelerating one plate. Although the steady-state Couette flow problem of a simple gas has been investigated by many authors for both linearized[4] and nonlinear cases,[5)-9)] there exist only a few investigations for the steady-state Couette flow problem of a gas mixture. Weinstein[10] treated the steady-state Couette flow problem of a binary gas mixture for both linearized and nonlinear cases by the two-component equivalents of both Grad's thirteen moment approximation and Liu and Lees' two-stream function.

The purpose of this paper is to study the transient Couette flow problem of rarefied binary gas mixtures to see how the flow field relaxes to the steady-state and what phenomena are observed in the unsteady process. It is also the purpose to present the steady-state solution, which is obtained from the long-time result, and to examine especially the effects of Knudsen number, mixture ratio, and gas-surface interaction on the flow field. The steady-state solution is compared only qualitatively with the results of Weinstein, since the parameters defined by Weinstein could not be understood clearly.

The method used in this investigation is the Monte Carlo method. This method has yielded the results[3] in good agreement with those of the Monte Carlo methods by Haviland and Lavin[11] for the case of

* Received 12th March, 1970.

** The First Aerodynamics Division.

*** The light species m_1 relaxes on the order of $(m_2/m_1)^{\frac{1}{2}}$ faster than the heavy species m_2 which again relaxes on the order of $(m_2/m_1)^{\frac{1}{2}}$ faster than the time of equilibration between the species.

heat transfer between parallel plates and by Perlmutter[9] for the case of Couette flow. Haviland and Lavin[12] developed the Monte Carlo method, where the phase space is divided into small cells and a test particle is followed through three molecular events; i.e., collision with another molecule, crossing an intercell division, and crossing a boundary. Bird[13] developed the direct simulation technique, where, in principle, the cell division is unnecessary and a large number of molecules are followed through the molecular events; i.e., molecular collisions and molecular drifts, by separating them. In the present method, the physical space is divided into macroscopically small cells, in which the test particles for each molecular event are followed through the event.

In the following the case of nonlinear problem, $M_i \geqslant 1$, is studied. Since the calculation of molecular collisions requires a large proportion of computing time, the present solution is limited to the range of Knudsen number $K_n \geqslant 0.1$ (from free molecular to transition flow regime).

2. MONTE CARLO METHOD

The physical space is divided into macroscopically small cells of volume ΔV, each of which is assumed to be such that, within its boundaries, the variation of the distribution function f_i of the i-th species is infinitesimal and the assumption of molecular chaos is valid.

The change in f_i in a cell during a time interval Δt is written as follows: neglecting terms of higher order than the first of Δt gives [see condition (5)]

$$f_i^{(n+1)}=f_i^{(n)}+\frac{\partial f_i^{(n)}}{\partial t}\Delta t\,, \tag{1}$$

in which

$$f_i^{(n)}=f_i(\boldsymbol{r},\ \boldsymbol{v},\ t)\,, \tag{1a}$$

$$f_i^{(n+1)}=f_i(\boldsymbol{r},\ \boldsymbol{v},\ t+\Delta t)\,, \tag{1b}$$

where $\boldsymbol{r}$, $\boldsymbol{v}$, and t are the spatial coordinate, the velocity, and the time, respectively. The term $\partial f_i^{(n)}/\partial t$ is given by the Boltzmann equation[14]

$$\frac{\partial f_i}{\partial t}=-\boldsymbol{v}\cdot\frac{\partial f_i}{\partial \boldsymbol{r}}-\boldsymbol{x}_i\cdot\frac{\partial f_i}{\partial \boldsymbol{v}}+\sum_j\frac{\partial_j f_i}{\partial t}, \tag{2}$$

and

$$\frac{\partial_j f_i}{\partial t}=\int (f_i' f_{j1}'-f_i f_{j1})\, g\, b\, db\, d\varepsilon\, d\boldsymbol{v}_1\,, \tag{2a}$$

where $m_i\boldsymbol{x}_i$ is the external force on a molecule of mass m_i, g is the relative speed of a collision pair, and b and ε are the collision parameters. Substituting Eq. (2) into Eq. (1) gives

$$\begin{aligned} f_i^{(n+1)}=f_i^{(n)}&+\sum_\alpha\frac{\Delta t}{(\tau_D)_{i\alpha}}\Delta_\alpha{}^{(D)}f_i^{(n)}\\ &+\sum_\alpha\frac{\Delta t}{(\tau_F)_{i\alpha}}\Delta_\alpha{}^{(F)}f_i^{(n)}\\ &+\sum_j\frac{\Delta t}{(\tau_C)_{ij}}\Delta_j{}^{(C)}f_i^{(n)}\,, \end{aligned} \tag{3}$$

where Greek subscripts denote vector components, Latin subscripts denote components of a mixture, and the operators are defined as follows:

$$\Delta_\alpha{}^{(D)}=-\frac{v_\alpha}{V_{i\alpha}}\frac{\partial}{\partial(r_\alpha/L_\alpha)}\,, \tag{3a}$$

$$\Delta_\alpha{}^{(F)}=-\frac{x_{i\alpha}}{F_{i\alpha}}\frac{\partial}{\partial(v_\alpha/V_{i\alpha})}\,, \tag{3b}$$

$$\Delta_j{}^{(C)}=\frac{\partial_j}{\partial(\bar{\nu}_{ij}t)}\,, \tag{3c}$$

in which $V_{i\alpha}$, L_α, $F_{i\alpha}$, and $\bar{\nu}_{ij}$ are the characteristic molecular velocity, the characteristic cell length, the characteristic force, and the mean collision frequency of the i-th species with the j-th in the cell, respectively. The characteristic times $(\tau_D)_{i\alpha}$; drift time, $(\tau_F)_{i\alpha}$; force time, and $(\tau_C)_{ij}$; collision time, are defined as follows:

$$(\tau_D)_{i\alpha}=L_\alpha/V_{i\alpha}\,, \tag{4a}$$

$$(\tau_F)_{i\alpha}=V_{i\alpha}/F_{i\alpha}\,, \tag{4b}$$

$$(\tau_C)_{ij}=1/\bar{\nu}_{ij}\,. \tag{4c}$$

The terms $\Delta_\alpha{}^{(D)}f_i$, $\Delta_\alpha{}^{(F)}f_i$, and $\Delta_j{}^{(C)}f_i$ are the order of f_i, and the time interval Δt should be

$$\Delta t \ll (\tau_D)_{i\alpha},\ (\tau_F)_{i\alpha},\ (\tau_C)_{ij}\,. \tag{5}$$

It is noted that the characteristic values $V_{i\alpha}$, L_α, $F_{i\alpha}$, and $\bar{\nu}_{ij}$ and, therefore, the characteristic times $(\tau_D)_{i\alpha}$, $(\tau_F)_{i\alpha}$, and $(\tau_C)_{ij}$ depend upon the cell and the time.

Equation (3) indicates that the change in f_i in the cell during Δt due to molecular drifts, that due to external forces, or that due to molecular collisions can be evaluated independently one another provided the condition (5) is satisfied. The three independent processes; i.e., molecular drifts, external forces, and molecular collisions, are carried out by the Monte Carlo method. A number of test particles, each of which has the velocity distribution $f_i^{(n)}/n_i$, are chosen for each process, where n_i is the number density defined by

$$n_i=\int f_i\, d\boldsymbol{v}. \tag{6}$$

Following the test particles for each process through the process during Δt yields the change in the distribution function $f_i^{(n)}$ due to the process. Each process is carried out simultaneously in all the cells. After the three processes are carried out, the new distribution function $f_i^{(n+1)}$ is obtained by adding the change in $f_i^{(n)}$ due to each process to $f_i^{(n)}$ [see Eq. (3)].

In actual calculations, it is convenient to note that Eq. (3) can be written as

$$f_{(K)}=f_{(K-1)}+\Delta^{(K)}f_{(K-1)}\,,\quad K=1,2,3, \tag{7}$$

where $f_{(0)}=f_i^{(n)}$, $f_{(3)}=f_i^{(n+1)}$, and $\Delta^{(K)}$ denotes the first order operator; i.e., $\sum_\alpha(\Delta t/(\tau_D)_{i\alpha})\Delta_\alpha{}^{(D)}$, $\sum_\alpha(\Delta t/(\tau_F)_{i\alpha})\Delta_\alpha{}^{(F)}$, or $\sum_j(\Delta t/(\tau_C)_{ij})\Delta_j{}^{(C)}$, and the terms of higher order than the first are neglected. Equation (7) indicates that following the test parti-

cles for the process (K) with the velocity distribution $f_{(K-1)}/n_i$, which are sampled from the previous test particles for the process $(K-1)$, through the process (K) yields the distribution function $f_{(K)}$.

The macroscopic moments in the cell are evaluated as follows: let $\phi_i(\boldsymbol{r}, \boldsymbol{v}, t)$ be a molecular property, then the moment $n_i\bar{\phi}_i$ defined by

$$\bar{\phi}_i(\boldsymbol{r}, t)=(1/n_i)\int \phi_i f_i\, d\boldsymbol{v}, \tag{8}$$

is evaluated by

$$\bar{\phi}_i=\sum\phi_i/N_i, \tag{8a}$$

where N_i is the number of test particles in the cell and the summation runs over the test particles. The rate of transfer of ϕ_i to the boundary is evaluated by

$$n_i\overline{\phi_i\boldsymbol{\xi}\cdot\boldsymbol{n}}=\sum\phi_i/\delta S\delta t, \tag{8b}$$

where $\boldsymbol{\xi}$ is the relative molecular velocity to the boundary, $\boldsymbol{n}$ is the unit vector normal to the boundary (directed from gas to boundary), $\sum\phi_i$ denotes the accumulated amount of ϕ_i on the element of area δS during an interval of time δt by the test particles for the molecular drift.

2.1 Molecular Drift

The test particles for the molecular drift with the number of $N_i^{(D)}$ in the cell ΔV are followed as follows, where each test particle is assumed to represent $n_i\cdot\Delta V/N_i^{(D)}$ particles.

(1) Spatial coordinate $\boldsymbol{r}$ is assigned to each test particle, and the test particle is drifted to the point $\boldsymbol{r}+\boldsymbol{v}\Delta t$, where $\boldsymbol{r}$ is assumed to be uniformly distributed in the cell ΔV.

(2) If a test particle collides with a boundary wall with a velocity relative to the wall $\boldsymbol{\xi}'$, the particle is reflected with a relative velocity $\boldsymbol{\xi}$, whose probability density function is the scattering probability function $P_i(\boldsymbol{\xi}|\boldsymbol{\xi}')$ expressed in the form

$$-\boldsymbol{\xi}\cdot\boldsymbol{n}f_i^-(\boldsymbol{\xi})=\int_{\boldsymbol{\xi}'\cdot\boldsymbol{n}>0} P_i(\boldsymbol{\xi}|\boldsymbol{\xi}')\boldsymbol{\xi}'\cdot\boldsymbol{n}f_i^+(\boldsymbol{\xi}')d\boldsymbol{\xi}', \quad \boldsymbol{\xi}\cdot\boldsymbol{n}<0, \tag{9}$$

where

$$f_i(\boldsymbol{\xi})=f_i^+(\boldsymbol{\xi})+[f_i^-(\boldsymbol{\xi})-f_i^+(\boldsymbol{\xi})]H(-\boldsymbol{\xi}\cdot\boldsymbol{n}), \tag{9a}$$

in which

$$H(X)=\begin{cases}0, & X<0\\ 1, & X>0,\end{cases} \tag{9b}$$

and $f_i(\boldsymbol{\xi})=f_i(\boldsymbol{r}_W, \boldsymbol{\xi}, t)$, where $\boldsymbol{r}_W$ is the position on the wall.

Because the present knowledge of the mechanism of gas-surface interaction is very far short of being able to provide $P_i(\boldsymbol{\xi}|\boldsymbol{\xi}')$, the following simple model is postulated:[15),16)]

$$P_i(\boldsymbol{\xi}|\boldsymbol{\xi}')=\alpha_i(\boldsymbol{\xi}')P_{iW}(\boldsymbol{\xi})+[1-\alpha_i(\boldsymbol{\xi}')]\cdot\delta(\boldsymbol{\xi}-\boldsymbol{\xi}'+2\boldsymbol{\xi}'\cdot\boldsymbol{n}\,\boldsymbol{n}), \quad \boldsymbol{\xi}\cdot\boldsymbol{n}<0, \ \boldsymbol{\xi}'\cdot\boldsymbol{n}>0, \tag{10}$$

where $\alpha_i(\boldsymbol{\xi}')$ is the molecular reflection coefficient, $\delta(X)$ is the Dirac delta function, and

$$P_{iW}(\boldsymbol{\xi})=-\frac{\boldsymbol{\xi}\cdot\boldsymbol{n}\exp[-\boldsymbol{\xi}^2/(2R_iT_W)]\alpha_i(\boldsymbol{\xi})}{\int_{\boldsymbol{\xi}'\cdot\boldsymbol{n}>0}\boldsymbol{\xi}'\cdot\boldsymbol{n}\exp[-\boldsymbol{\xi}'^2/(2R_iT_W)]\alpha_i(\boldsymbol{\xi}')d\boldsymbol{\xi}'}, \tag{10a}$$

in which $R_i=k/m_i$, k is the Boltzmann constant, and T_W is the wall temperature. It is noted that $\alpha_i(\boldsymbol{\xi}')=0$ for completely specular reflection and $\alpha_i(\boldsymbol{\xi}')=1$ for perfectly diffuse reflection.

(3) The procedures (1) and (2) are carried out simultaneously in all the cells.

2.2 External Force

The test particles for the external force with the number of $N_i^{(F)}$ in the cell ΔV are followed as follows:

(1) The velocity of the test particle $\boldsymbol{v}$ is changed to be $\boldsymbol{v}+\boldsymbol{x}_i\Delta t$.

(2) The procedure (1) is carried out simultaneously in all the cells.

2.3 Molecular Collision

A test cell of volume ΔV_t is taken in the cell ΔV with the condition

$$n_i=N_i^{(C)}/\Delta V_t, \tag{11}$$

where $N_i^{(C)}$ is the number of test particles for the molecular collision. The test particles are followed in the test cell as follows:

(1) During the interval of time $(t, t+\Delta t)$, a collision time interval Δt_c is assigned by the probability density function

$$P(\Delta t_c)=\nu_c\exp(-\nu_c\Delta t_c), \tag{12}$$

in which the collision between $(i, \boldsymbol{v})$ and $(j, \boldsymbol{v}_1)$ is assumed to occur independently with an equal probability during Δt, where $(i, \boldsymbol{v})$ denotes the specific class of the i-th species with a velocity in the interval $(\boldsymbol{v}, \boldsymbol{v}+d\boldsymbol{v})$, and the total collision frequency in the test cell ν_c is evaluated at time t, since the change in the distribution function f_i during Δt is small. The collision frequency ν_c is given by

$$\nu_c=(\Delta V_t/2)\sum_i\sum_j n_i\bar{\nu}_{ij}, \tag{13}$$

and

$$\bar{\nu}_{ij}=(1/n_i)\int d\boldsymbol{v}f_i\int d\boldsymbol{v}_1 f_{j1}\pi b_{\max}^2 g, \tag{13a}$$

in which $b_{\max}$ is the cutoff impact parameter.[3),12)] For the case of intermolecular force $F_{ij}=\kappa_{ij}/r^\nu$, where r is the distance between the molecules, $b_{\max}$ is given by [3),14)]

$$b_{\max}=\bar{b}_{\max}(\kappa_{ij}/\mu_{ij}g^2)^{1/(\nu-1)}, \tag{14}$$

where $\mu_{ij}=m_im_j/(m_i+m_j)$, and $\bar{b}_{\max}$ is the cutoff parameter. The collision frequency ν_c with a multiple integral is evaluated by the Monte Carlo method.

(2) At the time assigned by the procedure (1), a collision of test particles between $(i, \boldsymbol{v})$ and $(j, \boldsymbol{v}_1)$ is assigned by the collision probability function

$P_{(i,v)(j,v_1)}$ given by

$$P_{(i,v)(j,v_1)}=\Delta V_t f_i f_{j1} \pi b^2_{\max} g/2\nu_c , \quad (15)$$

and the velocities after collision are calculated by assigning the collision parameters b and ε through the probability density function $P(b)=2b/b^2_{\max}$ and $P(\varepsilon)=1/2\pi$, respectively.

(3) The procedures (1) and (2) are carried out until the accumulated time $\sum \Delta t_c$ exceeds Δt.

(4) The procedures (1)—(3) are carried out simultaneously in all the cells.

3. FORMULATION OF THE PROBLEM

3.1 Problem Description

The geometry of the Couette flow problem is shown in Fig. 1. Each component of a binary gas

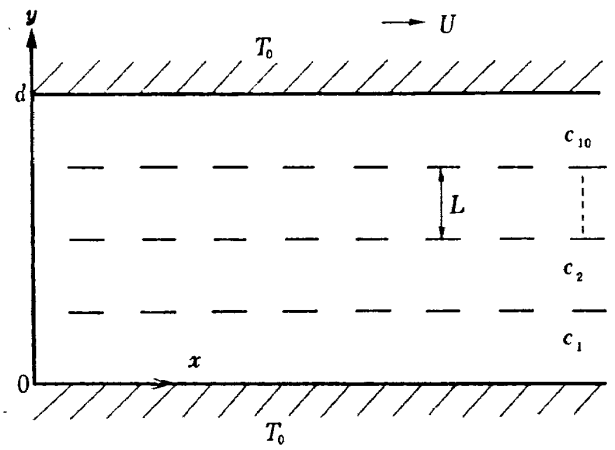

Fig. 1. Schematic flow field.

mixture with molecular mass m_i, number density n_{i0}, and temperature T_0 is initially equilibrium and at rest between two stationary infinite, parallel plates maintained at temperature T_0. The two plates are taken to be in the planes $y=0$ and $y=d$. At a given instant $t=0$, the upper plate $y=d$ is impulsively accelerated into uniform motion in its own plane with velocity U. The Maxwellian molecules are chosen as the molecular model; i.e., $\nu=5$. The force constant κ_{ij} is taken to be identical between the species; i.e., $\kappa_{ij}=\kappa$, and the case of no external forces is considered.

The subsequent motion is governed by the Boltzmann equation

$$\frac{\partial f_i}{\partial t}+v_y\frac{\partial f_i}{\partial y}=\sum_j \frac{\partial_j f_i}{\partial t} , \quad (16)$$

with the initial condition

$$f_i(y, v, 0)=\frac{n_{i0}}{(2\pi R_i T_0)^{3/2}}\exp\left(-\frac{v^2}{2R_iT_0}\right), \quad (17)$$

and the boundary conditions at $y=0$ and d are given by Eq. (9). The moments of interest are defined as follows:

$$n_i=\int f_i\, dv , \quad (18a)$$

$$\bar{v}_i=(1/n_i)\int v f_i\, dv , \; u_i=\bar{v}_{ix} , \quad (18b)$$

$$T_i=(1/3R_in_i)\int (v-\bar{v}_i)^2 f_i\, dv , \quad (18c)$$

$$P_{ixy}=m_i\int (v_x-\bar{v}_x)(v_y-\bar{v}_y) f_i\, dv , \quad (18d)$$

$$Q_{iy}=(m_i/2)\int v^2 v_y f_i\, dv , \quad (18e)$$

where $\bar{v}=\sum_i m_in_i\bar{v}_i/\sum_i m_in_i$. The drag coefficient C_{Di} and the energy-transfer coefficient C_{Ei} are defined by

$$C_{Di}=-P_{ixy}/\tfrac{1}{2}m_in_{i0}U^2 , \quad (18f)$$

$$C_{Ei}=-Q_{iy}/\tfrac{1}{2}m_in_{i0}C_{20}U^2 , \quad (18g)$$

where $C_{20}=(2R_2T_0)^{1/2}$.

The parameters to govern the flow field are chosen as follows: the mass ratio m_1/m_2, where the subscripts 1 and 2 refer to the light and the heavy species, respectively, the number fraction $X_i=n_{i0}/n_0$, where $n_0=\sum_i n_{i0}$, the reflection coefficient α_i, the plate Mach number $M=M_2$, where $M_i=U/(\gamma R_iT_0)^{1/2}$, γ is the ratio of specific heats, and $\gamma=5/3$ in the present case of monatomic gases, and the Knudsen number $Kn=\lambda/d$, where λ is the mean free path defined by $\lambda=(3\pi^{1/2}A_2(5)n_0)^{-1}(kT_0/\kappa)^{1/2}$ and $A_2(5)=0.436$ is the value of the scattering integral. The characteristic time t_0 is defined by $t_0=\lambda_2/C_{20}$, where λ_2 is the mean free path of the heavy species defined by $\lambda_2=(3\pi^{1/2}A_2(5)n_{20})^{-1}(kT_0/\kappa)^{1/2}$, and in the simple gas case; i.e., $m_1/m_2=1$, the characteristic time t_0 is defined by $t_0=\lambda/C_{20}$.

The free molecular solutions which are obtained by solving the collisionless Boltzmann equation are as follows: the distribution function for the case of $\alpha_i=1$ is

$$f_i=f_{i0}+(f_{iU}-f_{i0})H\left(t-\frac{y-d}{v_y}\right)H(-v_y) , \quad (19)$$

where

$$f_{i0}=\frac{n_{i0}}{(2\pi R_iT_0)^{3/2}}\exp\left(-\frac{v^2}{2R_iT_0}\right), \quad (19a)$$

$$f_{iU}=\frac{n_{i0}}{(2\pi R_iT_0)^{3/2}}\exp\left[-\frac{(v_x-U)^2+v_y^2+v_z^2}{2R_iT_0}\right]. \quad (19b)$$

The number density, the flow velocity, and the temperature are, respectively,

$$n_{fi}/n_{i0}=1 , \quad (20a)$$

$$u_{fi}/U=\frac{1}{2}\operatorname{erfc}\left(\frac{1-y/d}{t/t_{Di}}\right), \quad (20b)$$

$$T_{fi}/T_0=1+\frac{\gamma}{6}M_i^2\operatorname{erfc}\left(\frac{1-y/d}{t/t_{Di}}\right)\cdot\left[1-\frac{1}{2}\operatorname{erfc}\left(\frac{1-y/d}{t/t_{Di}}\right)\right], \quad (20c)$$

where t_{Di} is the drift time for a molecule to cross

the channel defined by $t_{Di}=d/(2R_iT_0)^{\frac{1}{2}}$, erfc$(X)$ is the complementary error function, and the subscript f denotes the free molecular value. The steady-state solutions $(t\to\infty)$ are

$$n_{fi}/n_{i0}=1, \tag{21a}$$

$$u_{fi}/U=1/2, \tag{21b}$$

$$T_{fi}/T_0=1+(\gamma/12)M_i^2. \tag{21c}$$

The coefficients C_{Di} and C_{Ei} are, respectively,

$$C_{Di}=(2/\pi\gamma)^{\frac{1}{2}}/M_i, \tag{21d}$$

$$C_{Ei}=(1/2\pi^{\frac{1}{2}})(m_2/m_i)^{\frac{1}{2}}. \tag{21e}$$

It is noted that the steady-state is established to be 90% in several drift times t_{Di} and the light species relaxes on the order of $(m_2/m_1)^{\frac{1}{2}}$ faster than the heavy species, since $t_{D1}/t_{D2}=(m_1/m_2)^{\frac{1}{2}}$, which is an epochal relaxation due to the molecule-surface collision [see Eq. (20)]. It is also noted that the separation phenomena between the species are observed, since the effect of the plate velocity U on the i-th species comes through the individual Mach number M_i [see Eq. (21)].

3.2 Application of the Monte Carlo Method

The channel between the plates is divided into small cells with width of L [see Fig. 1]. The characteristic times $(\tau_D)_{iy}$ and $(\tau_C)_{ij}$ are estimated as follows:

$$(\tau_D)_{iy}=L/C_i, \tag{22a}$$

$$(\tau_C)_{ij}=1/\bar{\nu}_{ij}, \tag{22b}$$

where the characteristic molecular velocity is taken to be $C_i=(2R_iT_i)^{\frac{1}{2}}$. The ratio $(\tau_D)_{iy}/(\tau_C)_{ij}$ is evaluated as

$$\frac{1}{\beta_{ij}}\frac{(\tau_D)_{iy}}{(\tau_C)_{ij}}=\frac{L}{d}\frac{1}{Kn}, \tag{23}$$

and is shown in Fig. 2, where β_{ij} is given by

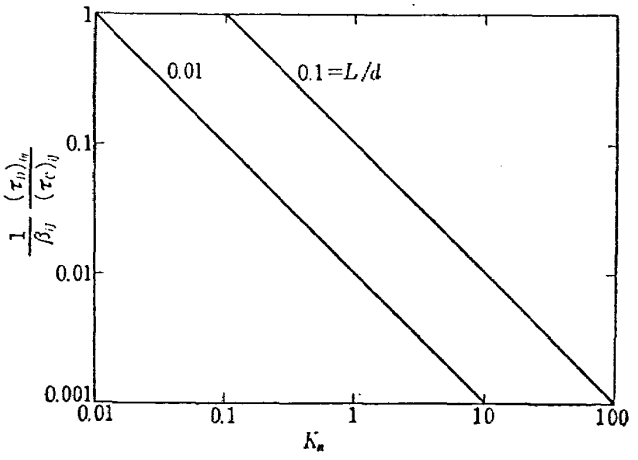

Fig. 2. Ratio of drift time to collision time.

$$\beta_{ij}=\frac{n_j}{n_0}\left(\frac{T_0}{T_i}\right)^{\frac{1}{2}}\left(\frac{m_i}{2\mu_{ij}}\right)^{\frac{1}{2}}. \tag{23a}$$

For the cell division $L/d\leqslant 0.1$, the drift time $(\tau_D)_{iy}$ is smaller than the collision time $(\tau_C)_{ij}$ in the present case of $Kn\geqslant 0.1$ and $m_i/m_j\leqslant 0(10)$, since it is expected that $\beta_{ij}\leqslant 0(1)$ for $Kn\geqslant 0.1$ and $m_i/m_j\leqslant 0(10)$ (which is verified from the results). Therefore, the time step Δt should be taken to be $\Delta t\ll(\tau_D)_{iy}$.

A HITAC 5020F computer is used in the calculations. The cells are denoted by $C_1, C_2, \cdots, C_{10}$ from the lower plate* [see Fig. 1]. It is noted that the macroscopic property X of a cell may be a mean value of X in the cell, $\overline{X}=(1/L)\int Xdy$, and the cell division L/d should be smaller in the case of a larger spatial variation. In Fig. 3(c), the mean values in a cell $\bar{u}_f$ and $\overline{T}_f$ are presented for comparison. The time step Δt is chosen to be $\Delta t/(\tau_D)_{f1}\sim 0.1$, where $(\tau_D)_{fi}=L/(2R_iT_{fi})^{\frac{1}{2}}$, since it is espected that $(\tau_D)_{fi}\lesssim(\tau_D)_{iy}(T_i\lesssim T_{fi})$ and $(\tau_D)_{f1}\leqslant(\tau_D)_{f2}$. The condition $\Delta t\ll(\tau_D)_{iy}$ is checked during calculations and the convergence is checked by comparing the difference of smaller time steps. The numbers of test particles of the i-th species are taken to be $N_i^{(D)}\sim N_i^{(C)}\sim 500$, which give the fluctuation of the result within several percent. The cutoff parameter $\bar{b}_{\max}$, which is used in the calculation of the total collision frequency ν_c, is taken to be $\bar{b}_{\max}=1.5$, which is sufficient for the actual calculations.[3),12)] Since a large proportion of computing time is spent for the molecular collision, the computing time increases as the Knudsen number decreases. For $Kn\sim 0.1$, the computing time is about 100 min.

4. RESULTS AND DISCUSSIONS

The Mach number is chosen to be $M=10$ in the nonlinear case. The results for $M=3$ are also presented for comparison. The mass ratio is chosen to be $m_1/m_2=0.1$, which is the value for a helium-argon mixture. The results for $m_1/m_2=1$; i.e., simple gas case, are also presented for comparison. The reflection coefficients are chosen to be $\alpha_1=\alpha_2=1$; i.e., perfectly diffuse reflection, and $\alpha_1=0$ and $\alpha_2=1$; i.e., completely specular reflection for the light species and perfectly diffuse reflection for the heavy species, which is expected for a disparate-mass gas mixture.[17)] The results for the mixture ratios $X_1=0$, 0.25, 0.5, and 0.75, and the Knudsen numbers $Kn=10$, 3, 1, 0.3, and 0.1, are presented.

4.1 Unsteady Solution

The transient development of the flow field is illustrated in Figs. 3 and 4.

The results for $\alpha_1=\alpha_2=1$ are presented in Fig. 3. Figure 3(a) shows the transient development of the velocity profile. The velocity increases first at the

* The cell division is taken to be L/d=0.1 (10 cells).

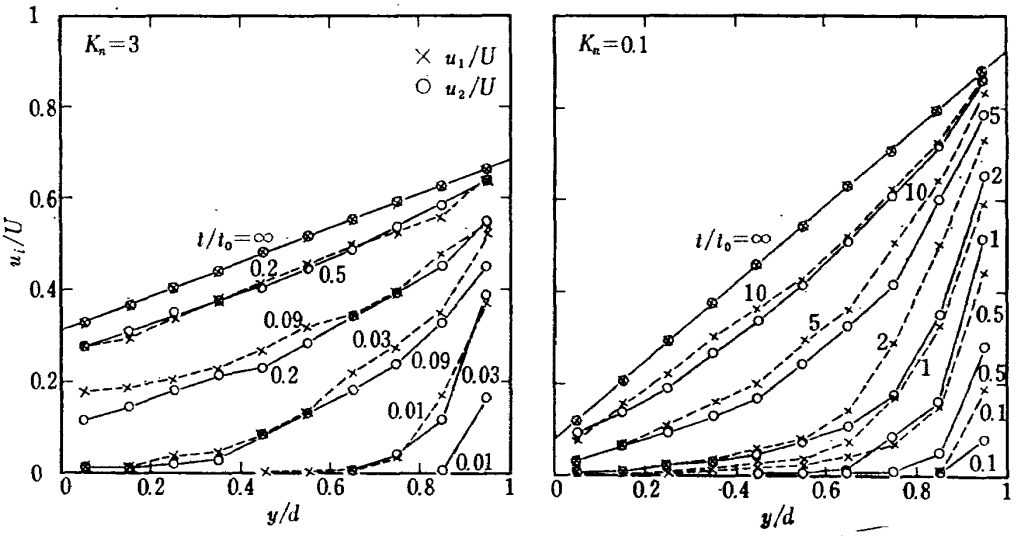

Fig. 3. Transient development of the flow field, M=10 and $\alpha_1=\alpha_2=1$; 3(a). Velocity profile, $m_1/m_2=0.1$ and $X_1=0.5$.

neighborhood of the moving plate and increases with time, asymptotically approaching the steady-state value. It takes a longer time for the velocity in the middle of the channel to reach the steady-state value than it does for the velocity near the plates. It is noted that the light species relaxes to the steady-state faster than the heavy species [see Fig. 3(a)-(b)]. The results for $\alpha_i=1$ indicate that the relaxation time for the i-th species to reach the steady-state is several drift times t_{Di} for $Kn\geqslant 0.1$, which is true in the case of free molecular limit [see Eq. (20)]. The light species relaxes on the order of $(m_2/m_1)^{\frac{1}{2}}$ faster than the heavy species, since $t_{D1}/t_{D2}=(m_1/m_2)^{\frac{1}{2}}$, which is an epochal relaxation due to the molecule-surface collision. It is interesting to note that the self-relaxation time $\tau_i=1/\nu_{ii}$ is proportional to $m_i^{\frac{1}{2}}$ (Grad's epochal relaxation[1]). As Kn decreases ($Kn\leqslant 0.1$), the molecule-molecule collision equilibrates the relaxation times of both species [see Fig. 3(a)-(b)].

Fig. 3(b) shows the transient development of the temperature profile. The temperature increases first at the neighborhood of the moving plate, asymptotically approaching the steady-state value. Of particular interest is the temperature "overshoot" over a steady-state value near the moving plate. This

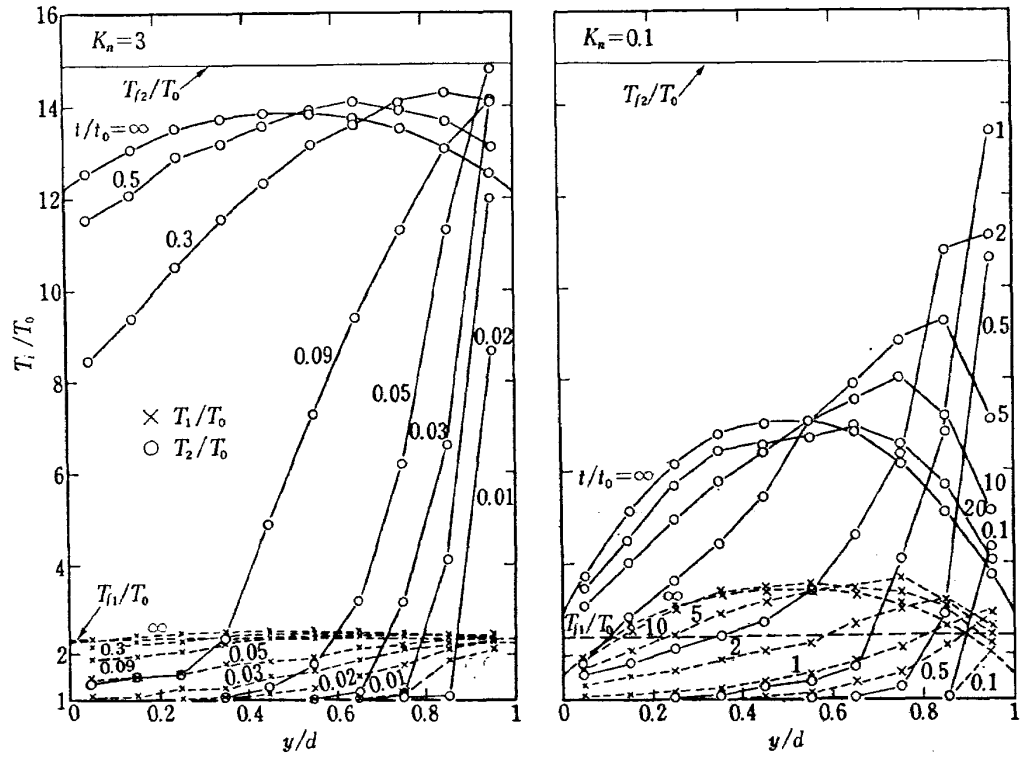

Fig. 3(b). Temperature profile, $m_1/m_2=0.1$ and $X_1=0.5$.

phenomenon is also observed in the case of simple gas,[8] where it is explained from the molecular viewpoint. Near the start of the motion, the molecule-moving plate collision surpasses the molecule-molecule collision. This regime is essentially the free molecular flow. This situation will continue until the molecule-molucule collision yields a larger value for the average directed motion of the gas, which decreases the energy of random motions or the temperature. Therefore, it is expected that the temperature "overshoot" is not observed in the free molecular limit [see Eq. (20)] and the maximum temperature does not exceed the steady-state free molecular temperature T_f. The variations of temperature and velocity of the cell C_{10} are shown in Fig. 3(c)

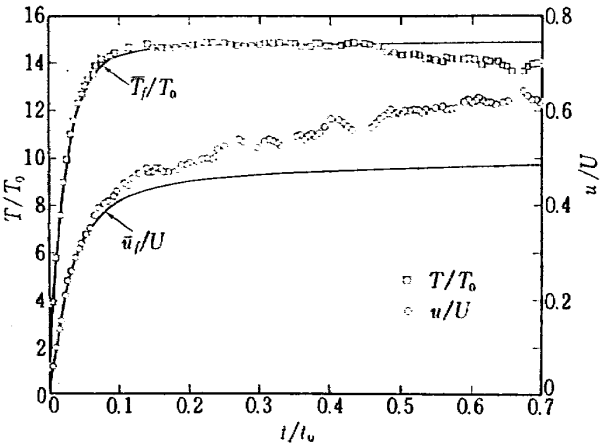

Fig. 3(c). Temperature and velocity of the cell C_{10} in comparison with free molecular temperature $\bar{T}_f$ and velocity $\bar{u}_f$, $m_1/m_2=1$ and $K_n=3$.

with the free molecular temperature $\bar{T}_f$ and the free molecular velocity $\bar{u}_f$. It is in fact observed that after the velocity exceeds $\bar{u}_f$ does the temperature begin to decrease. This situation is also true in the case of a gas mixture. However, as far as the light species is concerned, the collision with the heavy species increases the maximum temperature over the steady-state free molecular temperature T_{f1} [see Fig. 3(b)]. As Kn decreases, the "overshoot" phenomenon becomes evident and the "overshoot" region narrows [see Fig. 3(b)].

The number density also shows a complicated behavior: that near the moving plate undershoots and that near the stationary plate overshoots [see Fig. 3(d)]. This behavior is explained from the fact that the temperature near the moving plate increases faster than that near the stationary plate and the thermal velocity C_i near the moving plate is larger than that near the stationary plate ($C_i \propto T_i^{1/2}$). In the free molecular limit, the thermal velocity normal to the plate does not change and the number density is constant; i.e., $n_i/n_{i0}=1$ [see Eq. (20)].

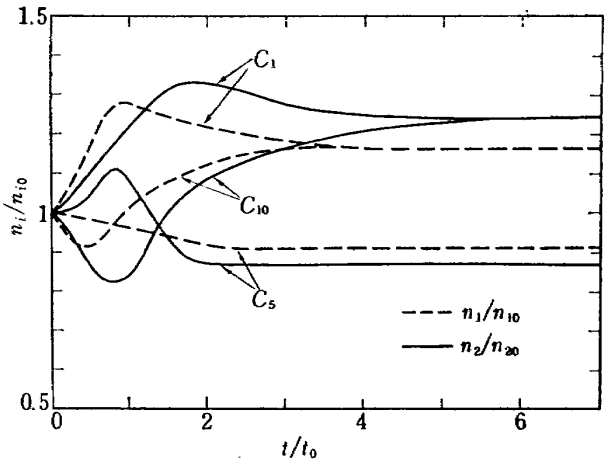

Fig. 3(d). Number density behavior, $m_1/m_2=0.1$, $X_1=0.5$, and $K_n=0.3$.

Figure 4 exhibits the characteristics of the case of $\alpha_1=0$ and $\alpha_2=1$. The steady-state solutions for $\alpha_i=1$ are also presented. Figure 4(a) shows the transient development of the velocity profile. The velocity slip of the light species is larger than that of the heavy species, as would be expected. The relaxation time of the light species is much greater than that for $\alpha_i=1$ and the epochal relaxation indicated in the case of $\alpha_i=1$ is not observed.

Of particular interest is the temperature behavior [see Fig. 4(b)]. The temperature of the light species T_1 increases to be much larger than that for $\alpha_i=1$ and the profile becomes flat. This phenomenon may be explained from the molecular viewpoint. The effect of the plate velocity on the light species

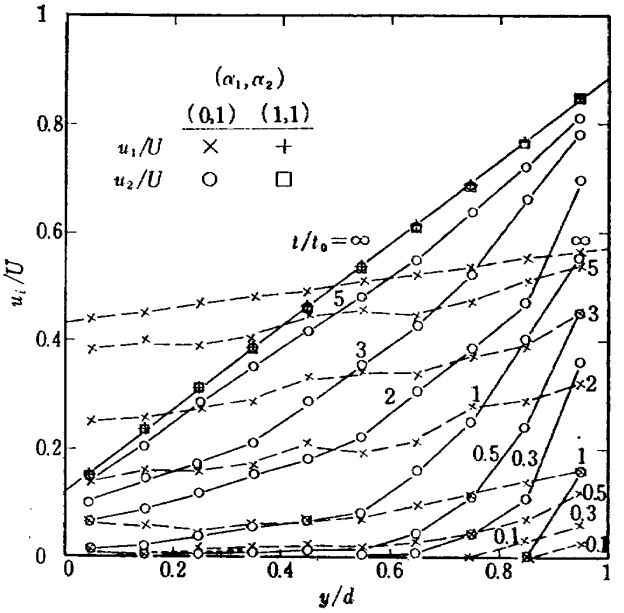

Fig. 4. Effect of gas-surface interaction on the flow field. Transient development of the flow field, $M=10$, $m_1/m_2=0.1$, $X_1=0.5$, and $K_n=0.3$;
4(a). Velocity profile.

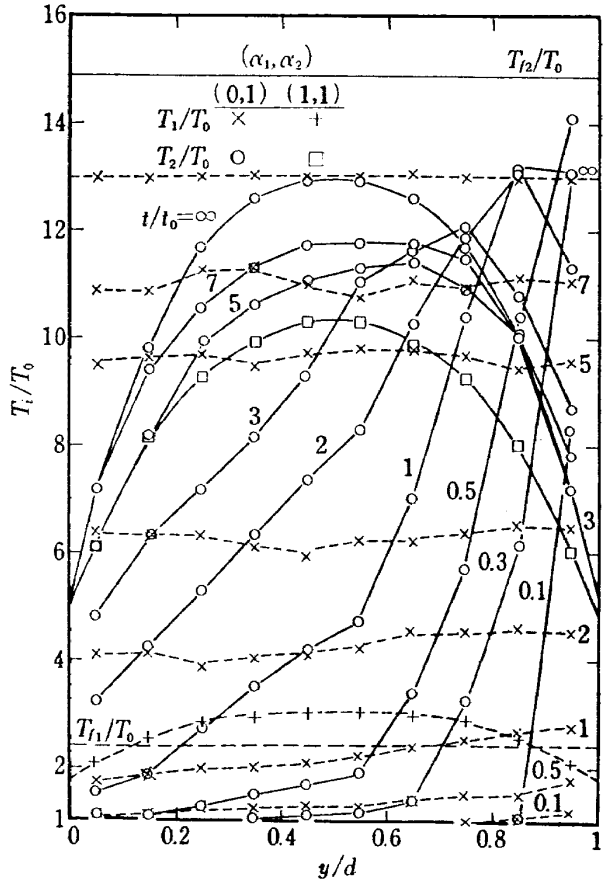

Fig. 4(b). Temperature profile.

comes through the collision with the heavy species, which increases not only the directed motion but also the random motion of the light species. Therefore, it is expected that the velocity slip and the temperature are larger than those for $\alpha_i=1$. The temperature of the heavy species T_2 overshoots, however, that of the light species T_1 does not overshoot, since there exists no free molecular flow regime for the light species (in the free molecular limit, the light species conserves the initial state).

4.2 Steady-State Solution

The flow field approaches asymptotically the steady-state, and the steady-state solutions are obtained from the long-time results. The typical results are presented in Figs. 5–8.

Figure 5 shows the profiles of temperature, velocity, and number density for $X_1=0.5$ and $\alpha_i=1$. The temperature profile is presented in Fig. 5(a). The temperatures T_1 and T_2 separate. This separation phenomenon is explained from the fact that the effect of the plate velocity U on the i-th species comes through the individual Mach number M_i as is shown in the free molecular case [see Eq. (21)]. As Kn decreases, T_2 decreases ($T_2 \leqslant T_{f2}$), T_1 near the plates also decreases ($T_1 \leqslant T_{f1}$), and T_1 in the middle of the channel increases ($T_1 \geqslant T_{f1}$), which

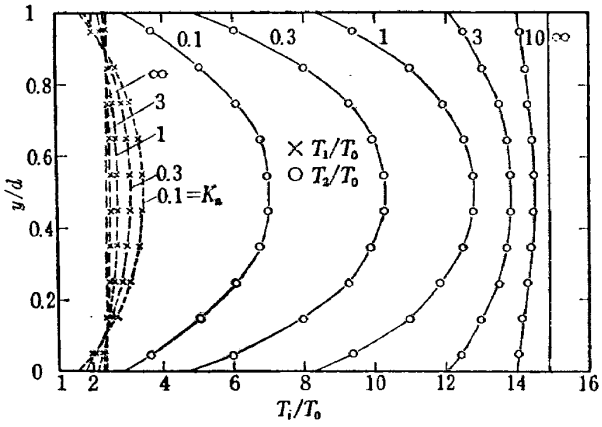

Fig. 5. Steady-state flow field, $m_1/m_2=0.1$, $X_1=0.5$, and $\alpha_1=\alpha_2=1$;
5(a). Temperature profile, $M=10$.

is due to the collision with the heavy species. As Kn decreases, T_1 and T_2 approach each other, since the molecule-molecule collision equilibrates the two temperatures. The qualitative comparison of the present results with those of Weinstein[10] by the two-component equivalents of both Grad's thirteen moment approximation and Liu and Lees' two-stream function indicates that the present solution yields qualitative agreement for the temperature profiles with that of the Liu and Lees' two-stream function approximation.

The velocity profile is presented in Fig. 5(b). The velocities u_1 and u_2 coincide with each other in the case of free molecular limit. As Kn decreases, the velocity slip decreases. It is interesting that u_1 and u_2 separate at $Kn\sim1$ and the velocity slip of the light species is larger than that of the heavy

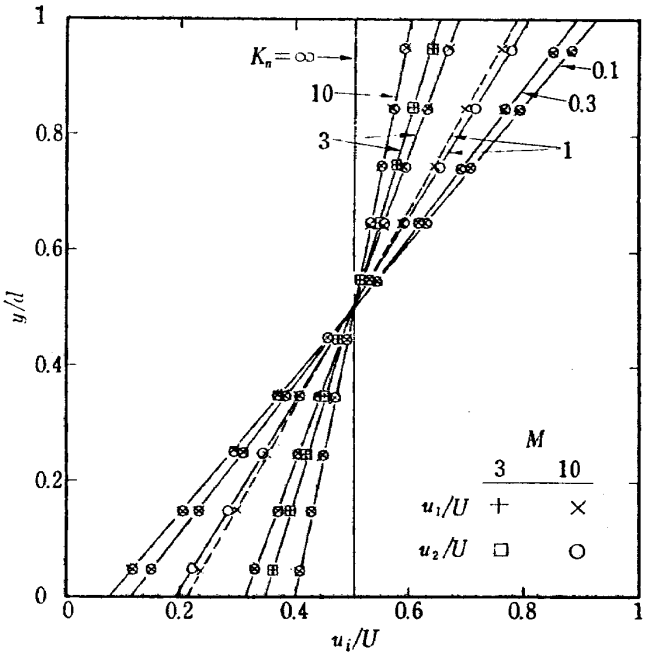

Fig. 5(b). Velocity profile.

species. This phenomenon is explained as follows. Since the Mach number is interpreted to be the ratio of the directed motion to the random motion; i.e., $M_i \sim U/(2R_iT_0)^{\frac{1}{2}}$, it is expected that the effect of the plate velocity U decreases as M_i decreases, which yields the increase of the velocity slip. Figure 5(b) demonstrates also the effect of the Mach number for $Kn=3$. The velocity slip for $M=3$ is in fact larger than that for $M=10$. Since $M_1<M_2$, it is expected that the velocity slip of the light species is larger than that of the heavy species. For $Kn<1$, the molecule-molecule collision equilibrates u_1 and u_2.

The number density profile is presented in Fig. 5(c). The number densities n_1/n_{10} and n_2/n_{20} coincide with each other in the free molecular limit.

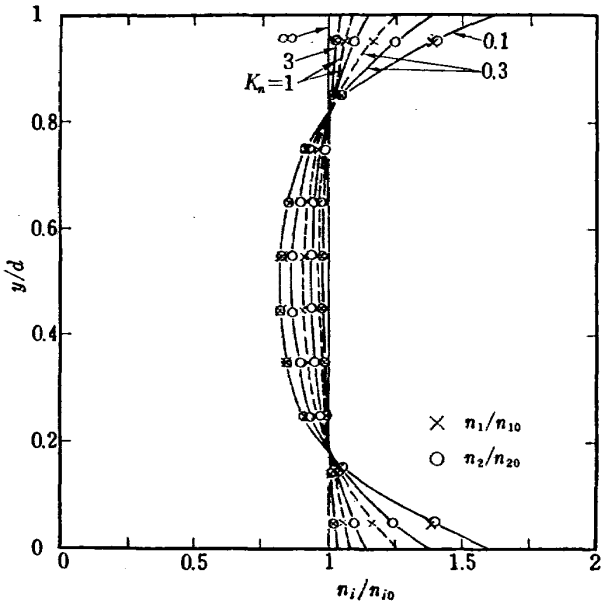

Fig. 5(c). Number density profile, $M=10$.

As Kn decreases, n_i/n_{i0} near the plates increases and that in the middle of the channel decreases. The separation between n_1/n_{10} and n_2/n_{20} is observed at $Kn\sim1$ and exhibits maximum at $Kn\sim0.3$ in agreement with the results of Weinstein.[10] For $Kn\leqslant0.1$, the molecule-molecule collision equilibrates n_1/n_{10} and n_2/n_{20}.

Figure 6 illustrates the effect of the mixture ratio X_i for $\alpha_i=1$. Figure 6(a) shows the effect of X_1 on the temperature. As X_1 increases, the temperatures T_1 and T_2 decrease as would be expected from $T_1<T_2$. The temperature decrease in the middle of the channel is larger than that near the plates.

Figure 6(b) shows the effect of X_1 on the velocity. As X_1 increases, the velocity slip increases as would be expected from $M_1<M_2$. It is noted that the separation between u_1 and u_2 is observed for

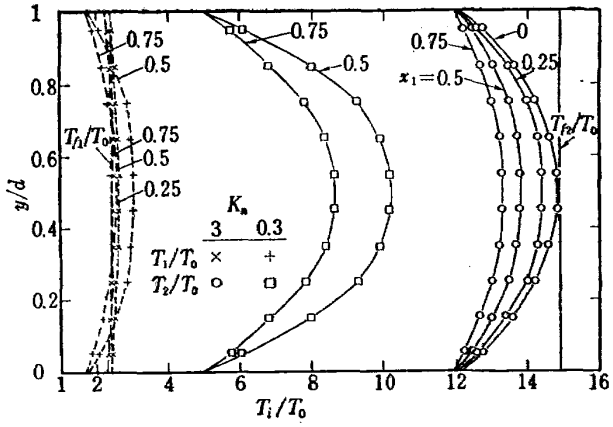

Fig. 6. Effect of mixture ratio on the flow field, $M=10$, $m_1/m_2=0.1$, and $\alpha_1=\alpha_2=1$; 6(a). Steady-state temperature profile.

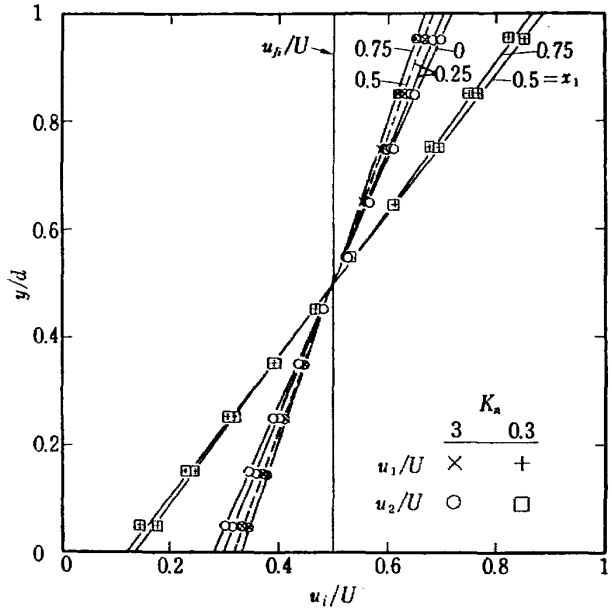

Fig. 6(b). Steady-state velocity profile.

$Kn\sim3$ and $X_1\sim0.25$, since the collision frequency between the light and the heavy species is small (the separation of number density n_i/n_{i0} is also observed for $Kn\sim3$ and $X_1\sim0.25$).

Figure 6 shows also the effect of the mass ratio m_1/m_2; i.e., the case of $X_1=0$ corresponds to the case of $m_1/m_2=1$ and arbitrary X_i. As m_1/m_2 decreases, the temperature decreases and the velocity slip increases as would be expected from $M_1/M_2=(m_1/m_2)^{\frac{1}{2}}$.

The results for $\alpha_1=0$ and $\alpha_2=1$ are presented in Figs. 4 and 7 for $Kn=0.3$ and $X_1=0.5$ in comparison with the case of $\alpha_i=1$. Figure 4(a) shows the velocity profile. The separation between u_1 and u_2 is evident and the velocity slip of the light species is larger than that of the heavy species as would be expected. The velocity slip of the light species is larger than that for $\alpha_i=1$ and u_2 is close to that for $\alpha_i=1$, which is also expected.

Figure 4(b) shows the temperature profile, which indicates the distinctive characteristics. The separation between T_1 and T_2 is evident and the profile of T_1 is flat. The temperature T_1 is much larger than that for $\alpha_i=1$ and T_2 is also larger than that for $\alpha_i=1$.

Figure 7 shows the number density profile. The separation between n_1/n_{10} and n_2/n_{20} is evident and the profile of n_1/n_{10} is flat in correspondence to that of T_1 [see Fig. 4(b)]. On the other hand, the profile of n_2/n_{20} exhibits a larger spatial variation than that for $\alpha_i=1$, which also corresponds to the profile of T_2 [see Fig. 4(b)].

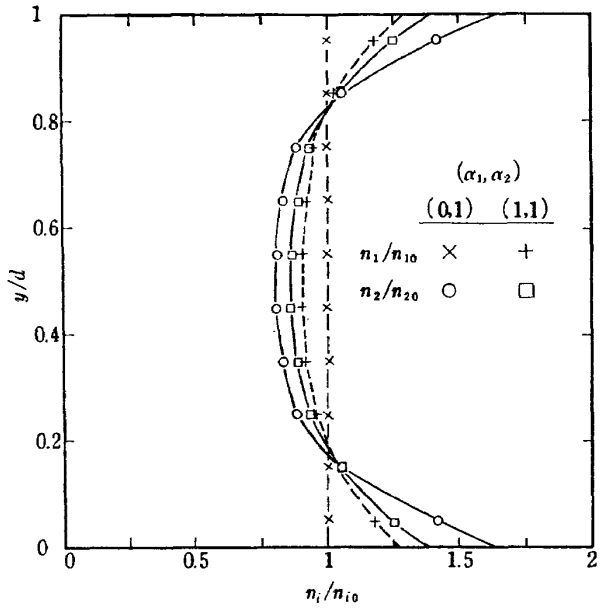

Fig. 7. Effect of gas-surface interaction on the flow field. Steady-state number density profile, $M=10$, $m_1/m_2=0.1$, $X_1=0.5$, and $Kn=0.3$.

The drag coefficient C_{Di} and the energy-transfer coefficient C_{Ei} at the plate are presented in Fig. 8. For $\alpha_i=1$, as Kn decreases the two coefficients decrease, and as X_1 increases those decrease. For $\alpha_1=0$ and $\alpha_2=1$, the coefficients C_{D1} and C_{E1} are zero, C_{D2} and C_{E2} are larger than those for $\alpha_i=1$, and the values for C_{D2} and C_{E2} at $Kn=0.3$ are larger than those of the free molecular limit.

5. CONCLUDING REMARKS

The transient Couette flow problem of rarefied binary gas mixtures has been studied for the nonlinear case, $M_i \geqslant 1$, by the Monte Carlo method. The flow field has been calculated for Maxwellian molecules and the range of Knudsen number $Kn \geqslant 0.1$. The present results show the fluctuations within several percent. The relaxation phenomena of a gas mixture with the boundary effects are observed. The long-time results yield the steady-state solutions.

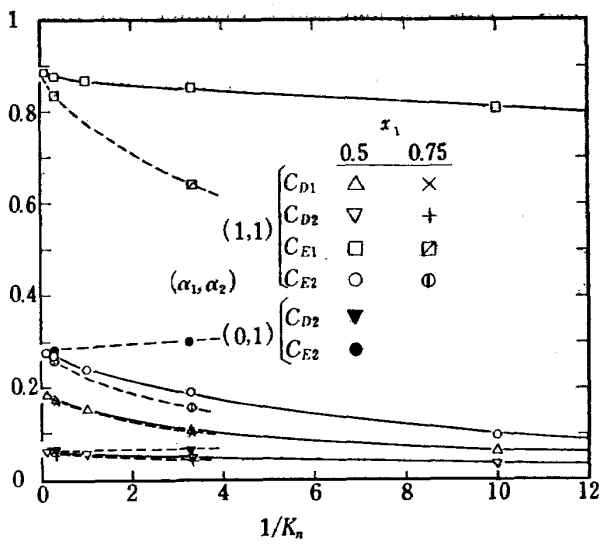

Fig. 8. Steady-state drag and energy-transfer coefficients at the plate, $M=10$ and $m_1/m_2=0.1$.

The results of the present investigation may be summarized in the following remarks:

(1) The relaxation time for the i-th species to reach a steady state is several drift times t_{Di} for $\alpha_i=1$, and the light species relaxes to the steady state faster than the heavy species (an epochal relaxation due to the molecule-surface collision).

(2) The temperature "overshoot" is observed near the moving plate for both light and heavy species for $\alpha_i=1$. The number density also shows a complicated behavior: that near the moving plate undershoots and that near the stationary plate overshoots.

(3) For $\alpha_1=0$ and $\alpha_2=1$, the relaxation time of the light species is much greater than that for $\alpha_i=1$ and the epochal relaxation is not observed. The temperature T_2 overshoots, however, T_1 does not overshoot. The temperature T_1 increases to be much larger than that for $\alpha_i=1$ and the profile becomes flat.

(4) The steady-state solutions indicate the separation phenomena between the species. The temperature separation is evident and the present solution yields qualitative agreement for the temperature profiles with that of the Liu and Lees' two-stream function approximation by Weinstein. The velocity separation is observed at $Kn\sim1$ for $X_1\sim0.5$ and $\alpha_i=1$, where the number density separation is also observed and exhibits maximum at $Kn\sim0.3$ in agreement with the result of Weinstein.

(5) The mixture ratio X_1 influences the flow field. As X_1 increases, the temperature decreases, the velocity slip increases, and both drag and energy-transfer coefficients decrease.

(6) The gas-surface interaction significantly in-

fluences the flow field. For $\alpha_1=0$ and $\alpha_2=1$, the velocity slip of the light species is larger than that for $\alpha_i=1$, T_1 is much larger than that for $\alpha_i=1$, and the profiles of T_1 and n_1/n_{10} are flat. The coefficients C_{D1} and C_{E1} are zero, however, C_{D2} and C_{E2} are larger than those for $\alpha_i=1$.

ACKNOWLEDGMENT

The author wishes to thank K. Ogawa, a member of the Rarefied Gas Dynamics Section in the 1st Aerodynamics Division, for assistance in the reduction of data.

REFERENCES

1) H. Grad; Rarefied Gas Dynamics (1960) pp. 100–138, Pergamon Press.
2) A. B. Huang and D. P. Giddens; Kinetic Theory of the Transient Couette Flow Problem, Phys. Fluids, Vol. 11 (1968) pp. 446–448.
3) K. Koura; Ph. D, thesis, University of Tokyo (1969): K. Koura and J. Kondo; Rarefied Gas Dynamics (1969) pp. 181–184, Academic Press.
4) D. R. Willis; Comparison of Kinetic Theory Analyses of Linearized Couette Flow, Phys. Fluids, Vol. 5 (1962) pp. 127–135.
5) C. Y. Liu and L. Lees; Rarefied Gas Dynamics (1961) pp. 391–428, Academic Press.
6) H. G. Weinstein and W. R. Schowalter; Plane Couette Flow of Rarefied Gases, Phys. Fluids, Vol. 10 (1967) pp. 332–344.
7) D. G. Anderson; Numerical Solutions of the Krook Kinetic Equation, J. Fluid Mech. Vol. 25 (1966) pp. 271–287.
8) A. B, Huang and D. L. Hartley; Nonlinear Rarefied Couette Flow with Heat Transfer, Phys. Fluids, Vol. 11 (1968) pp. 1321–1326.
9) M. Perlmutter; Rarefied Gas Dynamics (1967) pp. 455–480, Academic Press.
10) H. G. Weinstein; Rarefied Gas Dynamics (1967) pp. 535–554, Academic Press.
11) J. K. Haviland and M. L. Lavin; Application of the Monte Carlo Method to Heat Transfer in a Rarefied Gas, Phys. Fluids, Vol. 5 (1962) pp. 1399–1405.
12) J. K. Haviland; Methods in Computational Physics, Vol. 4 (1965) pp. 109–209, Academic Press.
13) G. A. Bird; Aerodynamic Properties of Some Simple Bodies in the Hypersonic Transition Regime, AIAA J. Vol. 4 (1966) pp. 55–60.
14) S. Chapman and T. G. Cowling; The Mathematical Theory of Non-Uniform Gases (1958), Cambridge University Press.
15) H. Grad; On the Kinetic Theory of Rarefied Gases, Commun. Pure Appl. Math. Vol. 2 (1949) pp. 331–407.
16) M. Epstein; A Model of the Wall Boundary Condition in Kinetic Theory, AIAA J. Vol. 5 (1967) pp. 1797–1800.
17) J. C. Crews; Scattering of Helium and Argon from the Cleavage Plane of Lithium Fluoride, J. Chem. Phys. Vol. 37 (1962) pp. 2004–2008.

TR-189 The Hybrid Simulation of Guided and Controlled Flight of Rocket	Hajime KOSHIICHI, Masao NAKA, Hidehiko MORI, Noboru OISHI, Akio KANMURI & Kōzō HONMA	Jan. 1970
TR-190 Interaction of Blunt Bodies in Supessonic Flow	Takashi TANI, Iwao KAWAMOTO, Seizo SAKAKIBARA, Junichi NODA & Jiro KONDO	Feb. 1970
TR-191 Drag Measurement in Nearly-Free-Molecule-Flow Regime	Akira ONJI, Kiyoshi YAMAMOTO	Feb. 1970

TECHNICAL REPORT OF NATIONAL AEROSPACE LABORATORY
TR-192T

航空宇宙技術研究所報告 192 号 (欧文)

昭和 45 年 3 月 発行

発行所 航空宇宙技術研究所
東京都調布市深大寺町 1,880
電話武蔵野三鷹(0422)44-9171(代表)

印刷所 株式会社 東京プレス
東京都板橋区桜川 2 丁目 27 の 12

Published by
NATIONAL AEROSPACE LABORATORY
1,880 Jindaiji, Chōfu, Tokyo
JAPAN

Printed in Japan